IEEE Photonics Journal
An IEEE Photonics Society Publication

Open Access

# Low-Complexity Time-Domain Averaging-Based DAC Clock Tone Leakage Compensation for Short-Reach PAM4 Transmission

Volume 12, Number 3, June 2020

Ming Chen, *Member, IEEE*
Long Zhang
Hui Zhou
Qinghui Chen

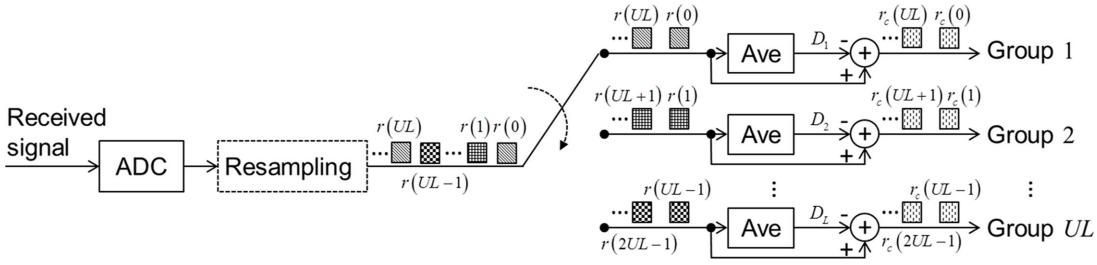


DOI: 10.1109/JPHOT.2020.2993046

# Low-Complexity Time-Domain Averaging-Based DAC Clock Tone Leakage Compensation for Short-Reach PAM4 Transmission

**Ming Chen** [1], ***Member, IEEE***, **Long Zhang** [1], **Hui Zhou** [2], **and Qinghui Chen** [3]

[1]School of Physics and Electronics, Hunan Normal University, Changsha 410081, China
[2]College of Information Science and Engineering, Hunan Normal University, Changsha 410081, China
[3]College of Computer and Communication, Hunan University of Technology, Zhuzhou 412007, China

*DOI:10.1109/JPHOT.2020.2993046*


Manuscript received March 30, 2020; revised April 25, 2020; accepted May 3, 2020. Date of publication May 7, 2020; date of current version June 1, 2020. This work was supported in part by the National Natural Science Foundation of China under Grants 61805079 and 61701180, and in part by the Scientific Research Fund of Hunan Provincial Education Department under Grants 18B026, 17C0957, and 18C0520. Corresponding author: Ming Chen (e-mail: ming.chen@hunnu.edu.cn).

**Abstract:** High sampling-rate digital-to-analog converters (DAC) are usually applied in optical fiber communication systems for the signal generation with advanced modulation formats such as four-level pulse amplitude modulation (PAM4). There exist various imperfections for high sampling-rate DACs. Clock tone leakage (CTL) is one of the imperfections and may seriously degrade the bit error rate (BER) performance, especially for single-carrier transmission systems. In this paper, we study a low-complexity time-domain averaging (TDA) based CTL compensation (TDA-CTLC) method for short-reach PAM4 transmission. By numerical simulation, we investigate the impacts of chromatic dispersion, CTL interference-to-signal power ratio (ISPR), and vertical resolution of the analog-to-digital converter on the BER performance. The results exhibit that the TDA-CTLC enabled PAM4 transmission system in the presence of a wide range of ISPR has a similar BER performance with the one without CTL interference. Moreover, we experimentally evaluate the compensation performance of the TDA-CTLC in a directly-modulated laser-based short-reach PAM4 transmission system. Up to $-4$ dB ISPR can be compensated with a slight BER performance degradation due to nonlinear distortions.

**Index Terms:** Clock tone leakage (CTL), Digital-to-analog converter (DAC), pulse amplitude modulation (PAM), time-domain averaging (TDA).

## 1. Introduction

Driven by upcoming high-speed services such as the Internet of Things, virtual reality, the fifth-generation applications, and cloud computing, the ever-increasing bandwidth demands continue to fuel the need for faster physical transmission technologies with low cost and power consumption in data center interconnects (DCI) and access networks [1], [2]. Unlike the long-reach transmission, the short-reach applications are more sensitive to cost. Therefore, intensity modulation with direct detection (IMDD) is a more promising solution in comparison to coherent detection. The on-off-keying (OOK) modulation with low spectral efficiency (SE) is widely applied in the conventional DCI

and passive optical networks (PON). It may be challenging to achieve a higher data rate beyond 100 Gbit/s per wavelength transmission with limited bandwidth and still maintain low-cost. Recently, many advanced modulation formats such as discrete multi-tone (DMT) [3]–[5] and four-level pulse amplitude modulation (PAM4) [6]–[8], have been employed to improve SE and reduce bandwidth requirements of the electrical and optical devices. Among these formats, PAM4 can be implemented with lower complexity and more power efficiency, which is going mainstream and has been incorporated into Ethernet standards such as IEEE 802.3bs and 802.3cd (400/200/100/50G) [9].

In the PAM4 transmitter, a high sampling-rate digital-to-analog converter (DAC) is usually required to generate the pulse-shaped signal. Time-interleaving (TI) [10] and analog bandwidth interleaving (ABI) [11] are two common techniques to achieve a high-speed DAC with multiple low-speed sub-DACs. However, there exist some imperfections for the DAC with a high sample rate at several tens of giga-samples per second (GSa/s) or more [12]. Clock tone leakage (CTL) is one of DAC imperfections, which can be regarded as an additive interference. In multi-carrier systems such as DMT, these subcarriers interfered by the CTL can be reserved to avoid degraded BER performance [13]. Nevertheless, this subcarrier reservation method will lead to reduced SE. In a PAM4 receiver, the CTL interference may seriously degrade the bit error rate (BER) performance due to its single-carrier modulation. To effectively compensate CTL, several methods have been proposed and investigated for optical fiber transmission systems. In [14], anti-phase pilot clock insertion and fast Fourier transform (FFT)-based frequency-domain CTL compensation methods are proposed and compared in a 400G single-carrier system with coherent detection. A rigid initial calibration is required to be performed to reduce the amplitude and phase mismatches to obtain the best mitigation efficiency. A 2-tap least mean square(LMS) based adaptive notch filter was also proposed and employed in both short-reach 100 Gbit/s PAM4 and DMT systems for CTL compensation (CTLC) [13], [15]. However, it requires massive multipliers for hardware implementation with high-level parallelism. In our previous work [16], two simple CTLC methods were proposed and experimentally investigated in a 100 Gbit/s DMT transmission system with 2-km single-mode fiber (SMF) link. It indicated that the proposed two methods could well compensate the CTL. The frequency-domain method was also explored in a short-reach DMT transmission system [17]. It was indicated that the CTL of DAC and the offset mismatch of the time-interleaved analog-to-digital converter (TI-ADC) could be compensated simultaneously. And the time-domain averaging (TDA) based CTLC method, which has also been applied for the compensation of the interference induced by TI-ADC offset mismatch [18], has lower hardware implementation complexity compared to the frequency-domain one.

In cost and power-sensitive application scenarios such as DCI and PON, it is preferable to use a simple and effective compensation method for the CTL of DAC. In this paper, we investigate the low-complexity online TDA-based CTLC method in a directly-modulated laser (DML) based short-reach PAM4 transmission system with IMDD for intra-DCI. We theoretically analyzed the operation principle of the proposed TDA-based CTL estimation and compensation method in detail. The convergence of the TDA-based CTL estimation is discussed. Moreover, the impacts of chromatic dispersion (CD), CTL interference-to-signal power ratio (ISPR) and vertical resolution of the analog-to-digital converter (ADC) on the BER performance are investigated by numerical simulations. Furthermore, we experimentally evaluate the compensation performance of the TDA-CTLC method in a wide range of ISPR.

The rest of the paper is arranged as follows. In Section 2, we theoretically analyze the CTL-induced impairments in a DML-based PAM4 transmission system and also describe the operation principle of the proposed TDA-CTLC. Simulation setup and results and discussion are presented in Section 3 and 4, respectively. Experimental verification is performed in Section 5. Conclusions are drawn in Section 6.

## 2. Theoretical Analysis and Operation Principle of the TDA-CTLC

Assume that there exists the CTL at $f_{CTL}$ Hz in a DAC with a high sampling rate of $K$ Sa/s. A Nyquist pulse shapes the mapped PAM symbols with equidistant levels. And the shaped discrete-time PAM4 signal $m(n)$ is converted to the baseband one $m(t)$ by the DAC. The converted signal with

the CTL $c(t)$ can be written by

$$s(t) = m(t) + c(t) \tag{1}$$

where $c(t) = B\cos(2\pi f_{CTL}t + \varphi_0)$, and $B$ and $\varphi_0$ represent the amplitude and the initial phase of the CTL, respectively. Here, we define the ISPR in decibel as

$$\text{ISPR} = 20\log_{10}\left(\frac{B}{\sqrt{2}\varepsilon}\right) \tag{2}$$

where $\varepsilon$ is the root mean square of $m(n)$. We will investigate the impact of different ISPRs on BER performance and discuss the compensation performance by using the proposed CTLC method.

Here, the baseband signal with the CTL is converted to an optical double-sideband signal by a DML. The envelope of the optical field after intensity modulation can be given by [19], [20]

$$E_{DML}(t) = A(t)^{1+j\alpha} \tag{3}$$

with

$$A(t) = \sqrt{P(t)} = A_0\sqrt{1+\sigma s(t)} \tag{4}$$

where $A(t)$ and $P(t)$ represent the instantaneous amplitude and power of the optical signal, respectively. $\sigma$ and $\alpha$ are a scaling constant and the alpha parameter of the DML (or linewidth enhancement factor), respectively. Based on the small-signal assumption of $\sigma s(t) \ll 1$, the first-order Taylor expansion of $E_{DML}(t)$ can be written as

$$E_{DML}(t) \cong A_0^{1+j\alpha}\left(1 + \frac{(1+j\alpha)}{2}\sigma s(t)\right) \tag{5}$$

The channel impulse response induced by CD of the dispersive SMF is $h_{CD}(t)$, and its frequency response is expressed as [21]

$$H_{CD}(f) = \exp\left[j\frac{\pi D z \lambda^2 f^2}{c}\right] \tag{6}$$

where $D$, $z$, $\lambda$ and $c$ are the dispersion parameter, transmission distance, operating wavelength, and speed of light in vacuum, respectively. $f$ denotes the low-pass equivalent frequency. After SMF transmission without taking fiber loss into account, Eq. (5) becomes

$$\begin{aligned} E_z(t) &= E_{DML}(t) \otimes h_{CD}(t) \\ &= A_0^{1+j\alpha}\left(1 + \frac{(1+j\alpha)}{2}\sigma s(t) \otimes h_{CD}(t)\right) \\ &= A_0^{1+j\alpha}\left(1 + \frac{\sigma}{2}s(t) \otimes h_z(t)\right) \end{aligned} \tag{7}$$

with the frequency response of $h_z(t)$

$$H_z(f) = \sqrt{1+\alpha^2}\exp\left[j\left(\frac{\pi D z \lambda^2 f^2}{c} + \arctan(\alpha)\right)\right] \tag{8}$$

A photodiode directly detects the received optical signal with the responsivity of $\upsilon$ and its output current can be written as

$$\begin{aligned} i(t) &= \upsilon|E_z(t)|^2 + w_{pd}(t) = \upsilon A_0^2 + \upsilon A_0^2\sigma s(t) \otimes \Re\{h_z(t)\} + \frac{\upsilon A_0^2\sigma^2}{4}|s(t) \otimes h_z(t)|^2 + w_{pd}(t) \\ &= \upsilon A_0^2 + \underbrace{\upsilon A_0^2\sigma m(t) \otimes h(t)}_{Desired\,Signal,\,m'(t)} + \underbrace{\upsilon A_0^2\sigma H(f_{CTL})c(t)}_{CTL@f_{CTL},\,c'(t)} + \underbrace{\frac{\upsilon A_0^2\sigma^2}{4}|m(t) \otimes h_z(t)|^2}_{SSBI} \\ &\quad + \underbrace{\frac{\upsilon A_0^2\sigma^2}{2}\Re\left\{(m(t) \otimes h_z(t)) \cdot (c(t) \otimes h_z^*(t))\right\}}_{SCBI} + \underbrace{\frac{\upsilon A_0^2\sigma^2(1+\alpha^2)}{4}c^2(t)}_{CTL@2\cdot f_{CTL},\,c''(t)} + w_{pd}(t) \end{aligned} \tag{9}$$

with

$$h(t) = \Re\{h_z(t)\} = \frac{1}{2}\left(h_z(t) + h_z^*(t)\right) \tag{10}$$

$$H(f) = \frac{1}{2}\left(H_z(f) + H_z^*(-f)\right) = \sqrt{1+\alpha^2}\cos\left(\frac{\pi D z \lambda^2 f^2}{c} + \arctan(\alpha)\right) \tag{11}$$

where the operator $\Re[x]$extracts the real part of a complex-valued number $x$. And the convolution and complex conjugation are represented by $\otimes$ and $*$, respectively. The first term of the right-hand side of Eq. (9) represents the direct current (DC) component. The second term is the desired signal distorted by CD. The third term and sixth term are the received CTLs at the frequencies of $f_{CTL}$ and $2f_{CTL}$, respectively. The fourth term is the signal-to-signal beating interference (SSBI) [22], and the fifth term is the signal-to-CTL beating interference (SCBI). The last term is the photodiode noise. Based on the small-signal assumption, the SSBI and the SCBI are small and can be regarded as one type of random additive noise. After DC blocking, Eq. (9) can be simplified as

$$\begin{aligned} r(t) &= m'(t) + c'(t) + c''(t) + w(t) \\ &= m'(t) + B'\cos\left(2\pi f_{CTL}t + \varphi'_0\right) + B''\cos\left(4\pi f_{CTL}t + \varphi''_0\right) + w(t) \end{aligned} \tag{12}$$

In general, the sampling rate of DAC is an integer ($L$) multiple of the frequency of the leaked clock tone [10]–[13], i.e., $L = K/f_{CTL}$. If the sampling rate of the ADC in the receiver is an integer multiple ($U$) of that of DAC, then the captured samples at the sampling instant $n/(UK)$ can be given by

$$r(n) = m'(n) + B'\cos\left(2\pi\frac{n}{UL} + \varphi'_0\right) + B''\cos\left(4\pi\frac{n}{UL} + \varphi''_0\right) + w(n) \tag{13}$$

where $n$ is a non-negative integer. As we can see that the received superimposed CTL is still a periodic sequence and there are $UL$ samples in each cycle. To estimate the CTL, we first divide the received samples $r(n)$ into $UL$ groups. And the $i$-th samples in the $l$-th group is $r(l-1+(i-1)UL)$. Since average values of the recovered PAM signal $m'(n)$ and additive noise $w(n)$ are both close to zeros, the result of the TDA operation on samples in the $l$-th group will be

$$D_l = \frac{1}{M}\sum_{i=1}^{M} r(l-1+(i-1)UL) \to B'\cos\left(2\pi\frac{l-1}{UL} + \varphi'_0\right) + B''\cos\left(4\pi\frac{l-1}{UL} + \varphi''_0\right) \tag{14}$$

The estimated CTL is a periodic sequence and the $l$-th sample in each cycle is $D_l$. The optimal value of averaging size $M$ will be discussed in section 4, to obtain an accurate estimate. Once CTL estimate is done, the $i$-th received sample with CTL in the $l$-th group can be compensated by

$$r_c(l-1+(i-1)UL) = r(l-1+(i-1)UL) - D_l \tag{15}$$

To achieve the hardware implementation of the TDA-CTLC algorithm as described in Eq. (14) and Eq. (15), only $UL$ real-valued accumulators and $UL$ dividers for the CTL estimation and $UL$ subtractors for the CTL compensation are required, respectively. However, the division by a constant $M$ can be reduced to a bit shift and addition or subtraction operations. Therefore, the complexity of the proposed TDA-CTLC is relative low.

The block diagram of the principle of the TDA-CTLC method is presented in Fig. 1. There three cases should be discussed for the use of the proposed method. Firstly, if the sampling rate of ADC is $U$ times that of the DAC, the resampling can be optionally performed for the $U > 1$ cases. If the sample is down-sampled to $K$ Sa/s and then the $U$ equals to 1. In our simulations, $U$ is 1 and the resampling is not required. Secondly, if the sampling rate of ADC is not an integer multiple of that of the DAC, then resampling should be performed before using the method. This is the case in our offline experimental verifications. Thirdly, if there is the sampling clock frequency offset (SCFO) induced by the clock mismatch between the transmitter and receiver, then an SCFO compensation such as digital interpolation, as shown in [23], should be done before the use of the proposed CTLC method. In this work, we focus on the former two cases.

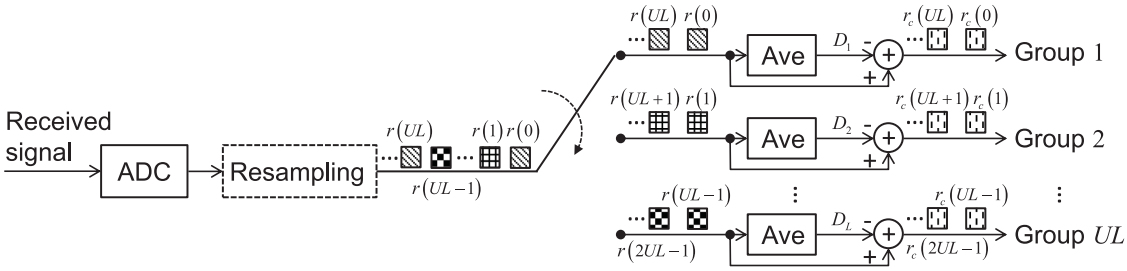


Fig. 1. The block diagram of the principle of the proposed TDA-CTLC method.

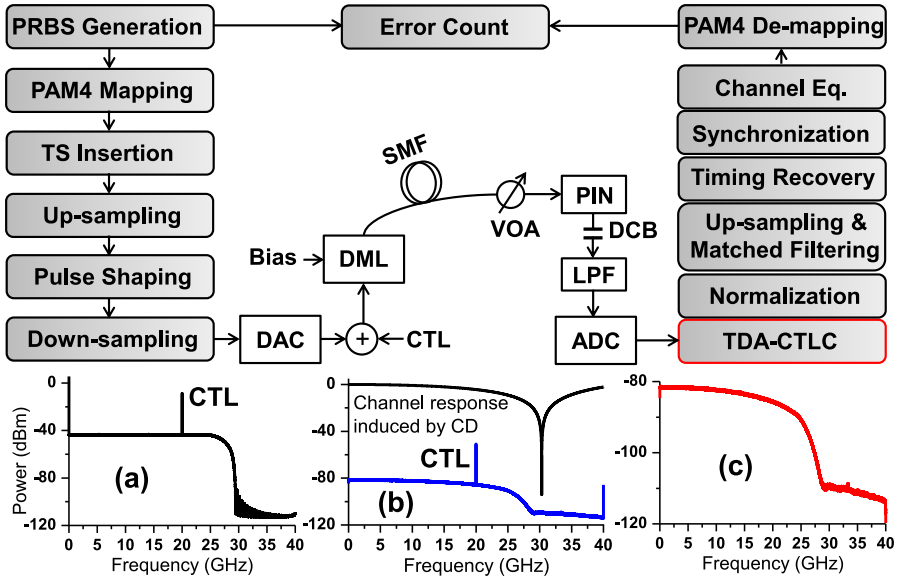


Fig. 2. The simulation setup of short-reach PAM4 transmission system with DAC CTL. Insets are the electrical spectra of (a) transmitted signal, (b) the received signal together with the CD-induced channel response, and (c) the signal after TDA-CTLC.

## 3. Simulation Setup

To evaluate the performance of the proposed TDA-CTLC, we establish the simulation setup of a short-reach PAM4 transmission system, as shown in Fig. 2. The digital signal processing (DSP) blocks for PAM signal generation and demodulation are also described for the simulation. In the transmitter DSP, a pseudo-random binary sequence (PRBS) with a period length of $2^{20}-1$ is generated for Gray-coded PAM4 symbol mapping with four equidistant levels. Two types of training sequence (TS) are also generated and appended at the beginning of the 1,200,000 data-carrying PAM4 symbols. The first TS consists of 1,024 two-level PAM (PAM2) symbols for symbol timing synchronization; while 2,048 PAM4 symbols are used as the second type TS to realize channel equalization. As a result, the total number of symbols in one frame is 1,203,072. Afterward, the frame signal is up-sampled by a factor of 3 and shaped by a square root raised cosine (SRRC) filter [15], [24], [25] with a roll-off factor of 0.1. The filter order of the SRRC is 1024 in this work. At last, the shaped signal is down-sampled to 1.5 samples per symbol and converted by a DAC operating at 80 GSa/s. The oversampling rate of DAC is 1.5 and the symbol rate is 53.3 GBaud. The bandwidth of the converted signal is 29.3 GHz. The CTL is emulated with a 20 GHz sine signal which superimposes on the frame signal. The corresponding spectrum is inserted in Fig. 2(a). The interfered signal drives a DML to generate the optical PAM4 signal. After a span of single-mode

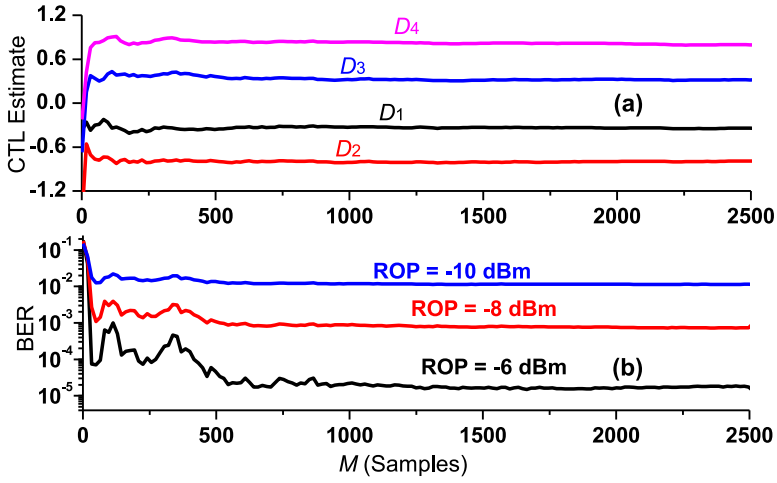


Fig. 3. The estimated CTL and BER performance versus averaging size $M$ ($K = 80$ GSa/s, $f_{CTL} = 20$ GHz, $U = 1$, and $L = 4$).

fiber transmission, a variable optical attenuator (VOA) is employed to change the received optical power (ROP) in front of a positive-intrinsic-negative (PIN) photodiode. The DC component of the recovered signal is removed by a DC block (DCB). And the out-of-band noise is suppressed with a low-pass filter (LPF). The filtered signal is sampled by an 80 GSa/s ADC and its spectrum is plotted in Fig. 2(b). The CD induced power fading is observed. According to Eq. (12), the power fading effect induced notch is located at around 30 GHz.

In the receiver DSP, the CTL is first estimated and compensated by using the proposed CTLC method for the interfered signal only. The spectrum of the compensated signal is shown in Fig. 2(c). Afterward, the compensated signal is normalized and up-sampled to 3 samples per symbol. And the same SRRC pulse shaping function is used for the matched filtering. Symbol timing recovery is performed with square timing algorithm [26] to find the optimal sampling instant in the symbol period. Symbol timing synchronization is realized with the first type of TS to identify the beginning of the PAM4 signal frame [27]. Channel equalization is realized by using the second type of TS-based and symbol-spaced 21-tap feed-forward equalizer (FFE). Note that tap coefficients of the FFE are adapted by using the second type of TS with the LMS algorithm. Once the estimation is done, the received data are equalized with the estimated FFE coefficients and then de-mapped with hard-decision. The step sizes for the FFE is 1e-2. A similar equalization method can be found in [28]. Subsequently, errors are directly counted over a frame signal with 2,400,000 information-bearing bits.

## 4. Simulated Results and Discussion

### *4.1 CTL Estimation and Compensation*

The interfered PAM4 signal with an ISPR of 0 dB is transmitted over 2-km SMF link, the recovered signal is sampled by the ADC with 8-bit resolution. The estimated CTL as a function of averaging size $M$ at the ROP of $-6$ dBm is presented in Fig. 3(a). It indicates the estimated CTL, which consists of $D_1$, $D_2$, $D_3$ and $D_4$, can reach stability when $M$ is more than 600. Note that the $M$ samples, for the estimation of each CTL component ($D_l$), are extracted from consecutive $MUL$ samples at an equal interval of $UL$, as shown in Fig. 1. Therefore, the corresponding convergence time should be 30 ns at the sample rate of 80 GSa/s. As we can see from Fig. 2(c), the leaked tone at 20 GHz is completely compensated. The measured BER performance at different ROPs with the CTLC method is also shown in Fig. 3(b). Fewer samples are required to reach the stable BER value as the ROP is reduced. This fact is that the dominant factor, which influences BER performance,

TABLE 1
Some Parameters Used in the Simulation

| Item | Parameter | Value | Unit |
|---|---|---|---|
| DAC | Sampling rate | 80 | GSa/s |
| | Resolution | Infinite | - |
| | Frequency of CTL | 20 | GHz |
| ADC | Sampling rate | 80 | GSa/s |
| | Resolution | 3 - 10 | bits |
| DML | Operating wavelength | 1550 | nm |
| | Output power | 7 | dBm |
| | Threshold current | 10 | mA |
| | Maximum current | 110 | mA |
| | Bias current | 60 | mA |
| | Alpha parameter | 1 | - |
| | Slope efficiency | 0.1 | W/A |
| | Linewidth | 1 | MHz |
| SMF | Length | 0, 1, 2 | km |
| | Attenuation | 0.2 | dB/km |
| | Dispersion | 17 | ps/nm/km |
| | Dispersion slope | 0.075 | $ps/nm^2/km$ |
| | Differential group delay | 0.2 | ps/km |
| PIN | Responsivity | 1 | A/W |
| | Thermal noise | 100e-24 | W/Hz |
| | Dark current | 10 | nA |
| LPF | Filter type | Butterworth | - |
| | 3-dB cut frequency | 30 | GHz |
| | Depth | 50 | dB |
| | Order | 6 | - |

is other system noises rather than CTL in the low ROPs. However, CTL is the main reason for the BER performance degradation in high ROPs, so more samples are required to obtain accurate CTL estimates. In the following discussions, $M$ is chosen to be 2500.

When the CTL is free and the ROP is $-6$ dBm, the recovered PAM4 symbols and its histogram after channel equalization are plotted in Fig. 4(a) and 4(d), respectively. The BER value is 1.5e-5. While there is CTL with the ISPR of 0 dB and no CTLC is applied, the receiver BER performance is seriously degraded as shown in Fig. 4(b). We can see the boundaries of the histogram of the PAM4 symbols are no longer clear and lots of recovered PAM4 symbols are near the hard-decision thresholds ($\pm 2$ and 0) from Fig. 4(e). This will lead to poor BER performance. The BER value of the recovered symbols shown in Fig. 4(b) is 7.6e-2. By using the CTLC method, the recovered PAM4 symbols and its histogram are shown in Fig. 4(c) and 4(f), respectively. We can see that the CTL can be well compensated, and the corresponding BER value is 1.54e-5, which is similar to the CTL-free case.

### *4.2 Impact of CD-Induced Power Fading*

We transmit the PAM signals with the ISPR of 0 dB and ISPR free over 0, 1 and 2 km SMF to investigate the impact of CD on the performance of the CTLC method. The measured BER performance as a function of ROP is presented in Fig. 5. A similar BER performance can be observed between the CTL free and CTLC enabled cases in different SMF transmission distances. With the increase of the SMF distance, the degraded BER performance is mainly attributed to the

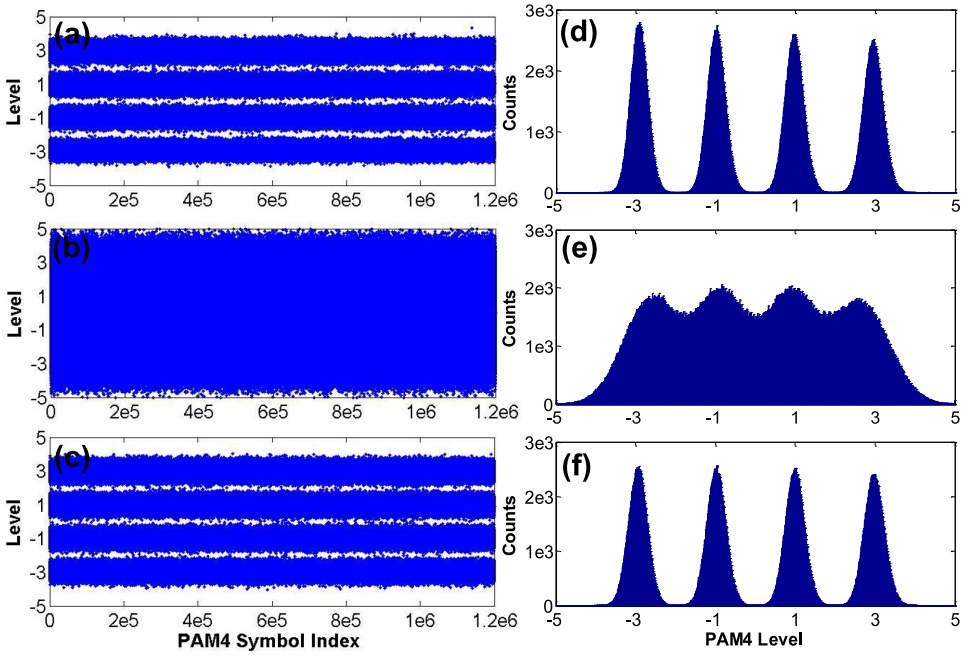


Fig. 4. The recovered PAM4 symbols after channel estimation and the corresponding histograms: (a), (d) w/o CTL; (b), (e) w/ CTL, and w/o CTLC; (c), (f) w/ CTL, and w/ CTLC.

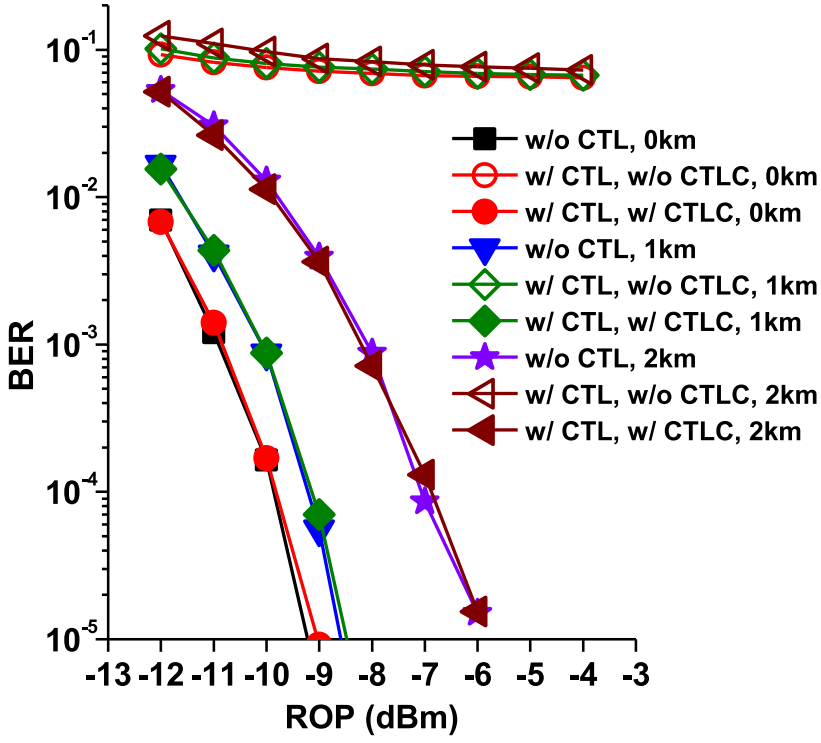


Fig. 5. The BER performance after different SMF distance transmission versus ROP.

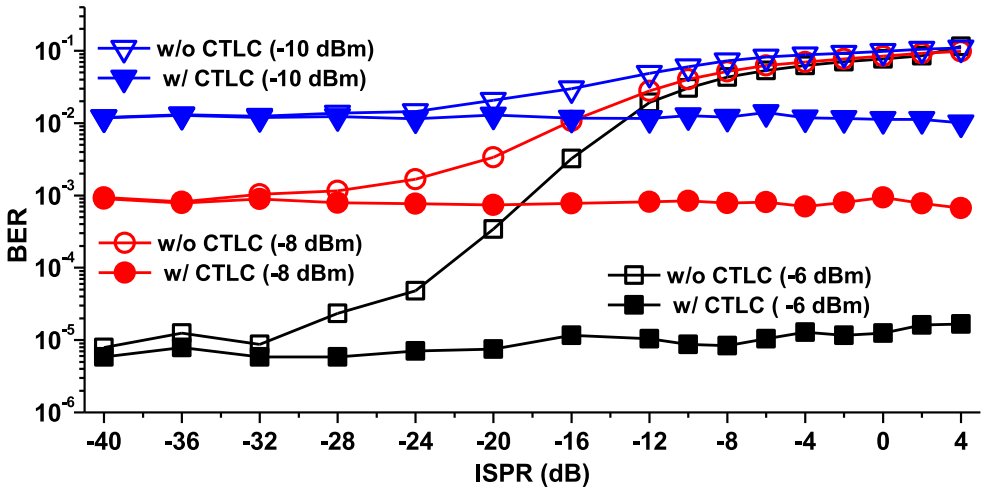


Fig. 6. The BER performance versus different ISPRs.

CD-induced power fading, as shown in Fig. 2(c). The BER performance without CTLC when ISPR is 0 dB is seriously deteriorated even through the SMF transmission distance is 0 km.

### 4.3 Impact of Different ISPRs

In this section, we change the power of the CTL to obtain the PAM4 signal with different ISPRs. The BER performance after 2-km SMF transmission at ROPs of −6, −8 and −10 dBm as a function of ISPR is shown in Fig. 6. The ISPR ranging from -40 to 4 dB is discussed. The BER values at ROPs of −6, −8 and −10 dBm after CTLC can be stabilized around 1e-5, 1e-3 and 1e-2, respectively. The BER performance gradually degrades as the ISPR increases in the absence of CTLC. When the ISPR is less than −32 dB, the impact of CTL on the BER performance is limited and can be ignored.

When the ISPR is set to the value larger than 4 dB, the peak clipping will be found in the DML and result in obvious BER performance degradation. We do not discuss this case. However, if the ROP is higher than −6 dBm, and then the BER is close to zero. In this case, we cannot effectively analyze the impact of large ISPR on the receiver performance according to the BER performance. Here we define the mean square error (MSE) between the recovered PAM symbol $r(n)$ and the reference symbol $t(n)$ as $10 \cdot \log_{10}(\sum_{n=1}^{N} [r(n) - t(n)]^2/N)$ in decibel, where $N$ is the total number of the transmitted symbols. The measured MSE after CTLC as a function of ISPR under different ROPs is presented in Fig. 7. It shows that the MSEs are stable over the range of ISPR from −40 to 4 dB in the case of low ROPs (−6, −8 and −10 dBm), which agrees well with the BER performance. It indicates that the CTL-induced SCBI is small and can be ignored when the ROP is low. However, we can see that the MSE gradually increases when the ROP is 2 dBm and ISPR is larger than −10 dB. In this case, the SCBI may be the main factor for the increased MSE.

### 4.4 Impact of ADC Resolution

To fully verify the feasibility and effectiveness of the CTLC method, we also investigate the impact of ADC vertical resolution ranging from 3 to 10-bit on the BER performance of the PAM4 receiver. The BER performance under three ROPs (−6, −8 and −10 dBm) and three ISPRs (CTL free, 0 and -16 dB) as a function of ADC resolution is given in Fig. 7. It indicates that the recovered signal with large ISPR of 0 dB is more sensitive to ADC quantization noise. And the slight BER performance degradation can be observed when ADC resolution is greater than 6-bit for the received signal at

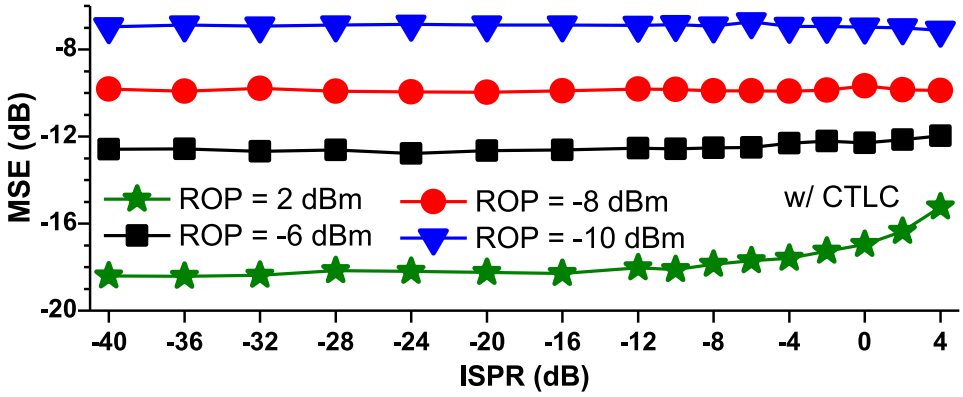


Fig. 7. The measured MSEs of the recovered PAM4 symbols with CTLC versus different ISPRs.

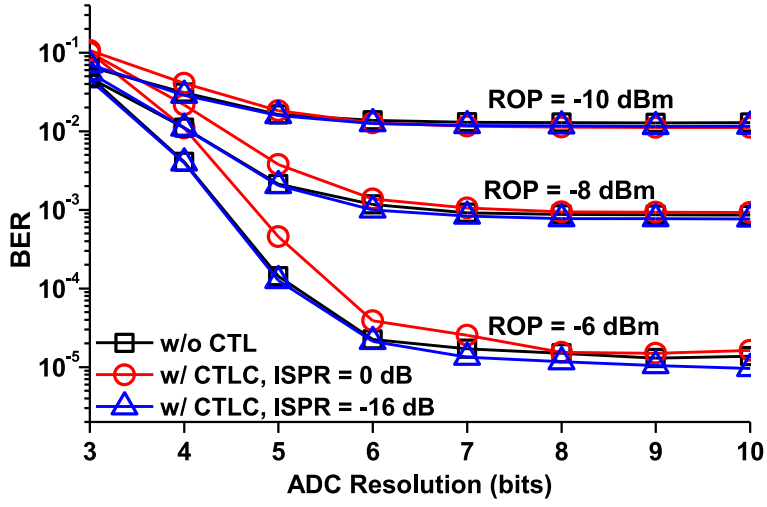


Fig. 8. The BER performance versus ADC resolution.

ROPs of −8 and −10 dBm. However, the vertical resolution of most commercial high sampling-rate ADC is 7-bit. Therefore, the impact of ADC resolution with 7-bit or more on the BER performance is negligible when the ISPR is up to 0 dB.

We also investigate the peak-to-average power ratio (PAPR) of the transmitted pulse-shaped PAM4 signal with CTL to further identify the possible reasons for the degraded BER performance in low ADC bit resolutions. The PAPR of the signal with different ISPRs of CTL is shown in Fig. 9. As we can see that the PAPR of the signal with a negligible CTL is about 8.7 dB. In the presence of ISPR of less than −6 dB, the PAPR slightly increases as ISPR increases. The maximum PAPR is about 9.7 dB at the ISPR of −6 dB. Afterward, the PAPR is gradually reduced when the ISPR is larger than −6 dB. The minimum PAPR is about 3 dB, which is equal to the theoretical PAPR of a cosine signal (or the CTL). In Fig. 8, we discuss the BER performance with ISPR of −16 and 0 dB. Here we can observe that the PAPRs for the signal with ISPRs of −16 and 0 dB are the same, and both of them are 9.3 dB. Thus, the ADC quantization noise maybe not the only factor for the degraded BER performance at the ISPR of 0 dB. Large quantization noise in low bit-resolution ADC will lead to an inaccurate estimation of CTL. And the larger residual CTL, compared to the case with the ISPR of −16 dB, is another factor for the degrade BER performance at the ISPR of 0 dB.

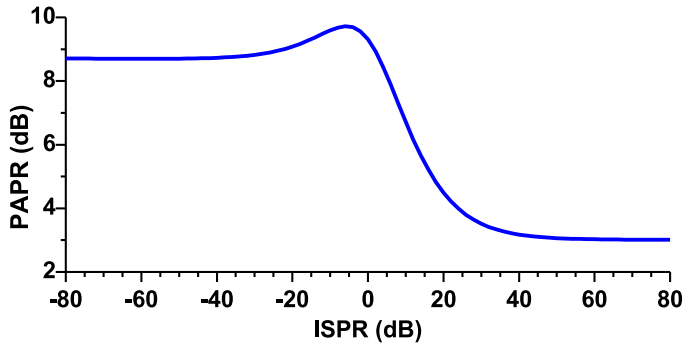


Fig. 9. The PAPR of the pulse-shaped PAM4 signal with different ISPRs of CTL.

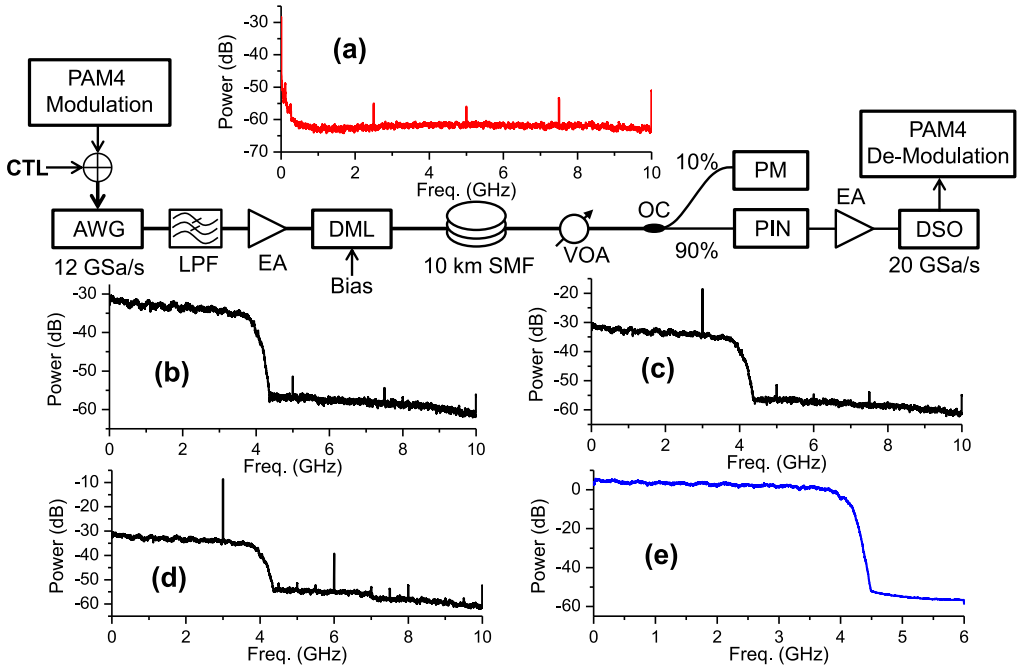


Fig. 10. Experimental setup. Insets are spectra of the received (a) noise when AWG turns off and PAM4 signal (b) without CTL, (c) with CTL (ISPR $= -10$ dB), (d) with CTL (ISPR $= 0$ dB), and (e) after CTLC.

## 5. Experimental Verification

In this section, we establish a proof-of-concept short-reach PAM4 transmission system to fully evaluate the feasibility of the proposed CTLC method. The block diagram of the experimental setup is illustrated in Fig. 10. The DSP algorithms included in PAM4 modulation/demodulation blocks are the same as those used in the simulation. We add a cosine waveform to the pulse-shaped PAM4 data in the digital domain to emulate the CTL at the frequency of 3 GHz. Afterward, the digital PAM4 signal with CTL is uploaded to a Tektronix arbitrary waveform generator (AWG, AWG7122C) operating at 12 GSa/s. The signal outputted from the AWG is first filtered by an LPF and then amplified with a broadband electrical amplifier (EA). It should be noted that the power of the PAM4 signal component remains the same for different ISPRs and only the power of CTL is changed in our experiment. A 10G-class commercial DML is driven by the amplified and interfered PAM signal and generates the optical signal. After 10 km SMF transmission, the received signal is attenuated by a VOA and then detected by a 10-GHz PIN photodiode after going through a 9:1 optical coupler

TABLE 2
Some Parameters Used in the Experiment

| Item | Parameter | Value | Unit |
|---|---|---|---|
| AWG | Sampling rate | 12 | GSa/s |
| | Resolution | 10 | bits |
| | Frequency of CTL | 3 | GHz |
| DSO | Sampling rate | 20 | GSa/s |
| | Resolution | 8 | bits |
| | Bandwidth | 20 | GHz |
| DML | Operating wavelength | 1556.3 | nm |
| | Output power | 2.3 | dBm |
| SMF | Length | 10 | km |
| | Attenuation | 0.18 | dB/km |
| | Dispersion | 17 | ps/nm/km |
| PIN | Bandwidth | 10 | GHz |
| | Coupling mode | AC | - |
| LPF | 3-dB bandwidth | 5.29 | GHz |
| | Depth | 30 | dB |
| EA | Bandwidth | 14 | GHz |

(OC). Meanwhile, the ROP is also measured online by using a power meter (PM). The second EA is used to amplify the detected baseband signal before realizing analog-to-digital conversion by employing a 20 GSa/s digital storage oscilloscope (DSO). Samples captured by the DSO are resampled to 12 GSa/s and further processed offline with DSP algorithms as the simulation does.

Several electrical spectra are analyzed and shown in Figs. 10(a)−(e). The spectrum of the received noise when the AWG turns off is shown in Fig. 10(a). It indicates that there are four peaks at the frequencies of 2.5, 5, 7.5 and 10 GHz. This may be attributed to the offset mismatch of time-interleaved ADC of the DSO. It also can be compensated by using the proposed TDA method [23]. However, the power of these frequency components is small and can be ignored in our experiment. The CTL-free spectrum is also shown in Fig. 10(b). The bit rate and bandwidth of the PAM4 signal are 16 Gb/s (12/1.5$*$2 Gb/s) and 4.4 GHz (12/1.5/2$*$1.1 GHz), respectively. The spectra of the received signal with ISPRs of −10 and 0 dB are presented in Figs. 10(c) and 8(d). We can see from Fig. 10(d) that several new small peaks at the frequencies of 4.5, 5.5, 6, 7 and 8 GHz are observed. It indicates that the converted signal with a large ISPR will suffer more nonlinear distortions from the DML and EA. This may lead to the degraded BER performance in the PAM4 receiver. The spectra of the compensated PAM signal is inserted in Fig. 10(e), where the CTL is well compensated by using the TDA-CTLC method. Some parameters of the devices used in our experiment are listed in Table 2.

We investigate the BER performance under different ISPR and ROPs to verify the compensation performance of the proposed TDA-CTLC method. The corresponding results are shown in Fig. 11. It indicates that up to −4 dB of ISPR can be compensated with slight BER performance degradation. In the simulation, nonlinear distortion from DML is not considered. However, the PAM4 signal with large ISPR will have more significant signal amplitude swing and suffer more nonlinear distortions from the DML and EA in our experiment, as shown in Fig. 10(d). Therefore, the BER performance is degraded obviously at high ROPs when ISPR is larger than −4 dB. Also, we compare the results with ANF-based CTLC proposed in [15] to that of the proposed TDA-CTLC in this work. In our experiment, the adaptation step size and amplitude of the reference signal for the ANF-CTLC are 1e-4 and 0.8, respectively. And the bandwidth of the ANF-CTLC is 1.536 MHz. As we can see from Fig. 11, a similar BER performance can be observed with these two CTLC methods.

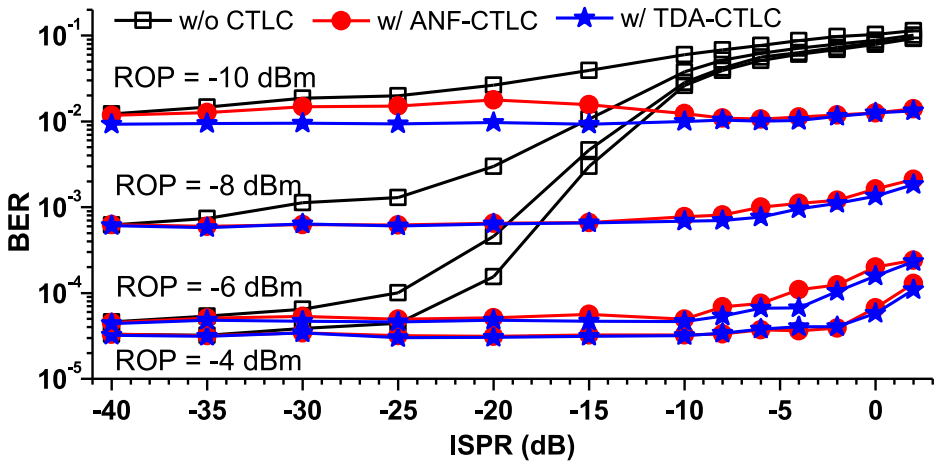


Fig. 11. The offline measured BER performance versus ISPR at different ROPs.

## 6. Conclusion

In this work, we investigated a low-complexity TDA-CTLC method for the short-reach PAM4 transmission system. The working principle of the CTL estimation and compensation was theoretically analyzed in detail. The convergence speed of the CTL estimation and its compensation performance were discussed. Moreover, the impacts of CD, ISPR and ADC vertical resolution on the BER performance were investigated by means of numerical simulation. The results exhibited that a similar BER performance can be achieved with the proposed CTLC method, compared to the CTL free case. Furthermore, the compensation performance is also experimentally investigated in a DML-based short-reach PAM4 transmission system. Up to $-4$ dB ISPR can be compensated with a slight BER performance degradation due to nonlinear distortions of the DML and EA. It is expected that the proposed CTLC method can be used to relax the design of high sampling-rate DAC for high-speed optical fiber transmission systems.

## References

[1] R. Giddings, "Real-time digital signal processing for optical OFDM-based future optical access networks," *J. Lightw. Technol.*, vol. 32, no. 4, pp. 553–570, Feb. 2014.
[2] N. Eiselt *et al.*, "First real-time 400G PAM-4 demonstration for inter-data center transmission over 100 km of SSMF at 1550 nm," in *Proc. Opt. Fiber Commun. Conf.*, 2016, Paper W1K.5.
[3] D. Zou, Z. Li, Y. Sun, F. Li, and Z. Li, "Computational complexity comparison of single-carrier DMT and conventional DMT in data center interconnect," *Opt. Express*, vol. 27, no. 12, pp. 17007–17016, 2019.
[4] D. Qian, N. Cvijetic, J. Hu, and T. Wang, "108 Gb/s OFDMA-PON with polarization multiplexing and direct detection," *J. Lightw. Technol.*, vol. 28, no. 4, pp. 484–493, Feb. 2010.
[5] L. Sun, J. Du, C. Wang, Z. Li, K. Xu, and Z. He, "Frequency-resolved adaptive probabilistic shaping for DMT-modulated IM-DD optical interconnects," *Opt. Express*, vol. 27, no. 9, pp. 12241–12254, 2019.
[6] D. Sadot, G. Dorman, A. Gorshtein, E. Sonkin, and O. Vidal, "Single channel 112Gbit/sec PAM4 at 56Gbaud with digital signal processing for data centers applications," *Opt. Express*, vol. 23, no. 2, pp. 991–997, 2015.
[7] J. Huo *et al.*, "Transmitter and receiver DSP for 112 Gbit/s PAM-4 amplifier-less transmissions using 25G-class EML and APD," *Opt. Express*, vol. 26, no. 18, pp. 22673–22686, 2018.
[8] E. El-Fiky, M. Chagnon, M. Sowailem, A. Samani, M. Morsy-Osman, and D. V. Plant, "168-Gb/s single carrier PAM4 transmission for intra-data center optical interconnects," *IEEE Photon. Technol. Lett.*, vol. 29, no. 3, pp. 314–317, Feb. 2017.
[9] S. M. R. Motaghiannezam, "Optical PAM4 signaling and system performance for DCI applications," in *Proc. Opt. Fiber Commun. Conf.*, San Diego, CA, USA, 2019, Paper M3A.1.
[10] H. Huang, J. Heilmeyer, M. Grözing, M. Berroth, J. Leibrich, and W. Rosenkranz, "An 8-bit 100-GS/s distributed DAC in 28-nm CMOS for optical communications," *IEEE Trans. Microw. Theory Techn.*, vol. 63, no. 4, pp. 1211–1218, Apr. 2015.

[11] C. Schmidt, C. Kottke, R. Freund, F. Gerfers, and V. Jungnickel, "Digital-to-analog converters for high-speed optical communications using frequency interleaving: Impairments and characteristics," *Opt. Express*, vol. 26, no. 6, pp. 6758–6770, 2018.
[12] M. Gustavsson, J. J. Wikner, and N. Tan, *CMOS Data Converters for Communications*. Berlin/Heidelberg, Germany: Springer Science & Business Media, Jan. 31, 2000.
[13] D. Zou *et al*., "Comparison of null-subcarriers reservation and adaptive notch filter for narrowband interference cancellation in intra-data center interconnect with DMT signal transmission," *Opt. Express*, vol. 27, no. 4, pp. 5696–5702, 2019.
[14] Y. Zhu, W.-R. Peng, Y. Cui, C. Kan, F. Zhu, and Y. Bai, "Comparative digital mitigations of DAC clock tone leakage in a single-carrier 400G system," in *Proc. Opt. Fiber Commun. Conf.*, Los Angeles, CA, USA, 2015, Paper Th2A.17.
[15] F. Li *et al*., "100 Gbit/s PAM4 signal transmission and reception for 2-km interconnect with adaptive notch filter for narrowband interference," *Opt. Express*, vol. 26, no. 18, pp. 24066–24074, 2018.
[16] M. Chen *et al*., "100-Gb/s DMT transmission for short-reach optical interconnect with DAC clock leakage compensation," *IEEE Photon. Technol. Lett.*, vol. 31, no. 22, pp. 1791–1794, Nov. 2019.
[17] M. Chen, L. Zhang, G. Liu, H. Zhou, Q. Chen, and C. Xiang, "Cancellation of subcarrier interference induced by DAC/ADC imperfections in short-reach DMT system," in *Proc. Asia Commun. Photon. Conf.*, 2019, Paper T4B.2.
[18] M. Chen, G. Liu, L. Zhang, H. Zhou, and Q. Chen, "Online digital offset mismatch compensation for high-speed time-interleaved ADC in real-time optical OFDM receiver," *Opt. Express*, vol. 27, no. 12, pp. 16650–16660, 2019.
[19] W. Shieh and I. Djordjevic, *OFDM for Optical Communications*. San Diego, CA, USA: Academic, 2009, ch. 7, pp. 280–282.
[20] C.-C. Wei, "Small-signal analysis of OOFDM signal transmission with directly modulated laser and direct detection," *Opt. Lett.*, vol. 36, no. 2, pp. 151–153, 2011.
[21] M. Sieben, J. Conradi, and D. E. Dodds, "Optical single sideband transmission at 10 Gb/s using only electrical dispersion compensation," *J. Lightw. Technol.*, vol. 17, no. 10, pp. 1742–1749, Oct. 1999.
[22] Z. Li *et al*., "Signal-signal beat interference cancellation in spectrally-efficient WDM direct-detection Nyquist-pulse-shaped 16-QAM subcarrier modulation," *Opt. Express*, vol. 23, no. 18, pp. 23694–23709, 2015.
[23] H. Zhou *et al*., "Joint clock recovery and feed-forward equalization for PAM4 transmission," *Opt. Express*, vol. 27, no. 8, pp. 11385–11395, 2019.
[24] J. Wei, Q. Cheng, D. G. Cunningham, R. V. Penty, I. H. White, and H. Griesser, "High performance 400 gigabit ethernet links using hybrid multiband CAP/QAM Scheme," in *Proc. Opt. Fiber Commun. Conf.*, 2015, Paper Th2A.65.
[25] M. Khalighi, S. Long, S. Bourennane, and Z. Ghassemlooy, "PAM- and CAP-based transmission schemes for visible-light communications," *IEEE Access*, vol. 5, pp. 27002–27013, 2017.
[26] M. Oerder and H. Myer, "Digital filter and square timing recovery," *IEEE Trans. Commun.*, vol. COM-36, no. 5, pp. 605–612, May 1988.
[27] M. Chen, J. He, and L. Chen, "Real-time optical OFDM long-reach PON system over 100-km SSMF using a directly modulated DFB laser," *J. Opt. Commun. Netw.*, vol. 6, no. 1, pp. 18–25, 2014.
[28] Z. Li, A. Tan, Y. Song, Y. Li, J. Chen, and M. Wang, "OOK-assisted adaptive equalization and timing recovery for PAM4 demodulation," *IEEE Photon. J.*, vol. 10, no. 2, Apr. 2018, Art. no. 7201607.